ELECTRONIC FILE AVAILABLE

Preprint
UCRL-JC-134821

A 3D Finite-Difference Frequency-Domain Code for Electromagnetic Induction Tomography

J.G. Berryman, N.J. Champagne II and H.M. Buettner

This article was submitted to
2nd International Symposium on Three Dimensional Electromagnetics
Salt Lake City, UT
October 27-29, 1999

U.S. Department of Energy
Lawrence Livermore National Laboratory

July 8, 1999

Approved for public release; further dissemination unlimited

DISCLAIMER

This document was prepared as an account of work sponsored by an agency of the United States Government. Neither the United States Government nor the University of California nor any of their employees, makes any warranty, express or implied, or assumes any legal liability or responsibility for the accuracy, completeness, or usefulness of any information, apparatus, product, or process disclosed, or represents that its use would not infringe privately owned rights. Reference herein to any specific commercial product, process, or service by trade name, trademark, manufacturer, or otherwise, does not necessarily constitute or imply its endorsement, recommendation, or favoring by the United States Government or the University of California. The views and opinions of authors expressed herein do not necessarily state or reflect those of the United States Government or the University of California, and shall not be used for advertising or product endorsement purposes.

This is a preprint of a paper intended for publication in a journal or proceedings. Since changes may be made before publication, this preprint is made available with the understanding that it will not be cited or reproduced without the permission of the author.

This report has been reproduced
directly from the best available copy.

Available to DOE and DOE contractors from the
Office of Scientific and Technical Information
P.O. Box 62, Oak Ridge, TN 37831
Prices available from (423) 576-8401
http://apollo.osti.gov/bridge/

Available to the public from the
National Technical Information Service
U.S. Department of Commerce
5285 Port Royal Rd.,
Springfield, VA 22161
http://www.ntis.gov/

OR

Lawrence Livermore National Laboratory
Technical Information Department's Digital Library
http://www.llnl.gov/tid/Library.html

A 3D Finite-Difference Frequency-Domain Code for Electromagnetic Induction Tomography

James G. Berryman, Nathan J. Champagne II, and H. Michael Buettner, Lawrence Livermore National Laboratory

Summary

We have developed a new 3D code for ElectroMagnetic Induction Tomography (EMIT) with intended applications to environmental imaging problems. We have used the finite-difference frequency-domain formulation of Beilenhoff *et al.* (1992) and the anisotropic PML (perfectly matched layer) approach (Berenger, 1994) to specify boundary conditions following Wu *et al.* (1997). PML deals with the fact that the computations must be done in a finite domain even though the real problem is virtually of infinite extent. The resulting formulas for the forward solver reduce to a problem of the form $\mathbf{A}x = y$, where $\mathbf{A}$ is a non-Hermitian matrix with real values off the diagonal and complex values along its diagonal. The matrix $\mathbf{A}$ may be either symmetric or nonsymmetric depending on details of the boundary conditions chosen (*i.e.*, the particular PML used for each application). The basic equation must be solved for the vector x (which represents field quantities such as electric and magnetic fields) with the vector y determined by the boundary conditions and transmitter location. Of the many forward solvers that could be used for this system, relatively few have been thoroughly tested for the type of matrix encountered in our problem. Our studies of the stability characteristics of the Bi-CG algorithm raised questions about its reliability and uniform accuracy for this application. We have found the stability characteristics of Bi-CGSTAB [an alternative developed by van der Vorst (1992) for such problems] to be entirely adequate for our application, whereas the standard Bi-CG was quite inadequate. We have also done extensive validation of our code using semianalytical results as well as other codes. The new code is written in Fortran 90 and is designed to be easily parallelized, but we have not yet tested this feature of the code. An adjoint method has also been developed for solving the inverse problem for conductivity imaging (for mapping underground plumes), and this approach, makes repeated use of the 3D forward modeling code we present here.

Introduction

Although electrical surveying techniques of both the current injection type and the magnetic field type have been well-known for many years (Telford *et al.*, 1976), efforts to turn these surveys into true 3D maps of subsurface physical properties have only been attempted in the last 10 to 20 years (Ramirez *et al.*, 1993; Tseng *et al.*, 1998). One of the reasons for this delay has been the necessity of large computer memories and fast computing machines, because it does not take a very large 3D forward modeling problem to swamp even today's most advanced computing platforms. A recent review of the state of the art in 3D EM modeling (Zhdanov *et al.*, 1997) demonstrated the limitations and lack of consensus on the best methods of computing EM fields in applications to inhomogeneous earth materials.

In this context, we have developed and continue to test and improve a new 3D code for application to electromagnetic induction tomography and to environmental imaging problems. We are using the finite-difference frequency-domain formulation of Beilenhoff *et al.* (1992) and the anisotropic PML (perfectly matched layer) approach (Berenger, 1994) to specify boundary conditions, following Wu *et al.* (1997). The present paper summarizes our progress to date on this code development.

Code Development

The goal of this code development effort is to produce an accurate and efficient forward simulation for EM fields that can then be easily used for inversion of ElectroMagnetic Induction Tomography (EMIT) field data. The FDFD (finite-difference frequency-domain) formulation presented here is an extension to lossy media of a method developed for lossless media by Beilenhoff *et al.* (1992). The mesh truncation approach uses an anisotropic absorbing PML (perfectly matched layer) following the ideas of Berenger (1994) and Sacks *et al.* (1995). The absorbing regions have material parameters similar to those proposed by Kuzuoglu *et al.* (1996). The code is written in Fortran 90, and portability to various high performance computing platforms has been one of our design criteria throughout its development.

Finite-difference, frequency-domain formulation

To develop a system of equations to determine the electric and magnetic fields within a volume, the integral form of Maxwell's curl equations (Ampère's and Faraday's laws),

$$\oint_C \mathbf{H} \cdot d\boldsymbol{\ell} = j\omega \int_S (\overline{\boldsymbol{\epsilon}} \cdot \mathbf{E}) \cdot \hat{\mathbf{n}}\, dS + \int_S \mathbf{J} \cdot \hat{\mathbf{n}}\, dS \quad (1)$$

and

$$\oint_C \mathbf{E} \cdot d\boldsymbol{\ell} = -j\omega \int_S (\overline{\boldsymbol{\mu}} \cdot \mathbf{H}) \cdot \hat{\mathbf{n}}\, dS - \int_S \mathbf{M} \cdot \hat{\mathbf{n}}\, dS, \quad (2)$$

are used. Here $\mathbf{J}$ is the impressed electric current density, $\mathbf{M}$ is the impressed magnetic current density, both $\overline{\boldsymbol{\epsilon}}$ and

$\overline{\mu}$ are diagonal dyads, and C is the boundary of the open surface S. The integrals in (1) and (2) are applied to discrete elements (rectangular blocks) within the volume using the following relations:

$$\int_{-a/2}^{a/2} \mathbf{f} \cdot d\boldsymbol{\ell} \rightarrow a f_m \tag{3}$$

and

$$\int_{-a/2}^{a/2} \int_{-b/2}^{b/2} \mathbf{f} \cdot \hat{\mathbf{n}}\, dS \rightarrow ab f_m, \tag{4}$$

where f_m is a center value associated with the mth cell shown in Figure 1. Note that the discrete electric field

Table 1: Cells surrounding the $m = \text{cell}(i,j,k)$ cell.

$d = \text{cell}(i-1,j,k)$	$u = \text{cell}(i+1,j,k)$
$l = \text{cell}(i,j-1,k)$	$r = \text{cell}(i,j+1,k)$
$f = \text{cell}(i,j,k-1)$	$b = \text{cell}(i,j,k+1)$

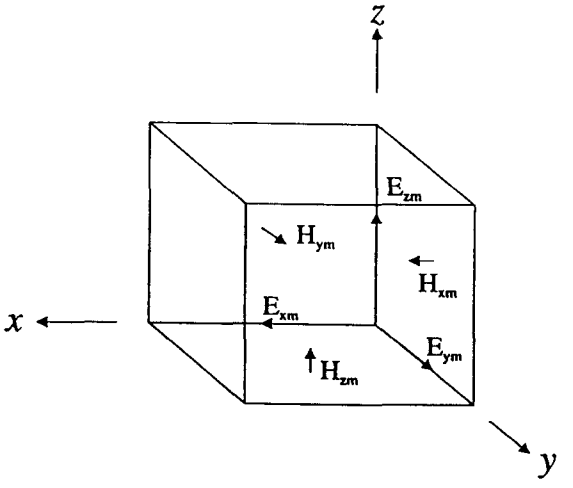

Fig. 1: The field quantities associated with the mth cell (i,j,k).

is located at the center of an edge and the discrete magnetic field flows through the centroid of a face. Also, the mth cell is normally referred to as cell(i,j,k), but for notational convenience, a cell mapping using symbols such as u, d, l, r, f, b (for up, down, left, right, front, back) to specify the six cells surrounding the mth cell is used. This mapping is presented in Table 1. Cells other than the six cells adjacent to the six faces may also be labelled using the same mapping. For example, relative to cell m, cell df is cell$(i-1,j,k-1)$ and cell dlb is cell$(i-1,j-1,k+1)$.

The discretized form of (1) and (2) results in an equation for each field component. The resulting equations are cumbersome; however, presenting each expression using matrices provides a compact form. Thus, using quantities defined in the Appendix, (1) and (2) become

$$\boldsymbol{A}^T \boldsymbol{D}_{\bar{\ell}}\, \vec{h} = j\omega\epsilon_0 \boldsymbol{D}_{A\epsilon}\, \vec{e} + \boldsymbol{D}_{\bar{A}}\, \vec{j} \tag{5}$$

and

$$\boldsymbol{A}\boldsymbol{D}_{\ell}\, \vec{e} = -j\omega\mu_0 \boldsymbol{D}_A\, \boldsymbol{D}_{\mu}\, \vec{h} - \boldsymbol{D}_A\, \vec{m}, \tag{6}$$

respectively. The apparent lack of symmetry in the pair of equations (5) and (6) arises from differences in the method of discretizing ϵ and μ on the staggered grid (see the Appendix for the details). Solving for the magnetic field (in order to eliminate it from the equations) in (6) and then substituting the result into (5) yields

$$\boldsymbol{A}^T \boldsymbol{D}_{\bar{\ell}}\, \boldsymbol{D}_{\mu}^{-1}\, \boldsymbol{D}_A^{-1}\, \boldsymbol{A}\boldsymbol{D}_{\ell}\, \vec{e} - k_0^2 \boldsymbol{D}_{A\epsilon}\, \vec{e} = -j\omega\mu_0 \boldsymbol{D}_{\bar{A}}\, \vec{j} - \boldsymbol{A}^T \boldsymbol{D}_{\bar{\ell}}\, \boldsymbol{D}_{\mu}^{-1}\, \vec{m}, \tag{7}$$

which has a form entirely analogous to that commonly used in finite element codes, *i.e.*,

$$\nabla \times \left(\overline{\mu}_r^{-1} \cdot \nabla \times \mathbf{E}\right) - k_0^2 \overline{\epsilon}_r \cdot \mathbf{E} = -j\omega\mu_0 \mathbf{J} - \nabla \times \overline{\mu}_r^{-1} \cdot \mathbf{M}, \tag{8}$$

even though our goal here is to develop a finite difference code.

A commonly observed problem in numerical computations of Maxwell's equations arises due to a possible resonance at zero frequency. If this occurs, the resulting matrix has an eigenvalue at zero and therefore is not positive definite and not invertible. For the geometries considered here, the fields for resonant frequency of 0 Hz are generated only by electric charge within the volume. Such charges may develop as an artifact of numerical roundoff when evaluating the vector wave equation — especially at lower frequencies. This problem is avoided by eliminating any charge within the volume using a term analogous to

$$\nabla\left[\nabla \cdot (\overline{\epsilon}_r \cdot \mathbf{E})\right] = \mathbf{0}. \tag{9}$$

This is achieved by starting from Gauss's law for the electric field in integral form,

$$\int_V \nabla \cdot (\overline{\epsilon}_r \cdot \mathbf{E})\, dV = \oint_S (\overline{\epsilon}_r \cdot \mathbf{E}) \cdot \hat{\mathbf{n}}\, dS = 0, \tag{10}$$

to arrive at the discretized matrix expression

$$\left[\boldsymbol{D}_{\ell}^{-1} \boldsymbol{D}_{A\epsilon}^{*} \boldsymbol{B}^T \left(\boldsymbol{D}_{V\epsilon\epsilon}^{-1} \boldsymbol{B} \boldsymbol{D}_{A\epsilon}\right)\right] \vec{e} = \vec{0}, \tag{11}$$

where the matrices in parenthesis arise from discretizing (10) while the remaining matrices in the square bracket arise from discretizing (9) after the application of an integral identity. When (11) is added to (7), the result is

$$\left(\boldsymbol{A}^T \boldsymbol{D}_{\bar{\ell}}\, \boldsymbol{D}_{\mu}^{-1}\, \boldsymbol{D}_A^{-1}\, \boldsymbol{A}\boldsymbol{D}_{\ell} + \boldsymbol{D}_{\ell}^{-1} \boldsymbol{D}_{A\epsilon}^{*} \boldsymbol{B}^T \boldsymbol{D}_{V\epsilon\epsilon}^{-1} \boldsymbol{B} \boldsymbol{D}_{A\epsilon} - k_0^2 \boldsymbol{D}_{A\epsilon}\right) \vec{e} = -j\omega\mu_0 \boldsymbol{D}_{\bar{A}}\, \vec{j} - \boldsymbol{A}^T \boldsymbol{D}_{\bar{\ell}}\, \boldsymbol{D}_{\mu}^{-1}\, \vec{m}. \tag{12}$$

However, a more symmetric form is obtained by multiplying through by $D^{1/2}$ and then rewriting (12) as

$$(D_\ell^{1/2} A^T D_{\tilde{\ell}} D_\mu^{-1} D_A^{-1} A D_\ell^{1/2} + D_\ell^{-1/2} D_{A\epsilon}^* B^T D_{V\epsilon\epsilon}^{-1} B D_{A\epsilon} D_\ell^{-1/2} - k_0^2 D_{A\epsilon}) D_\ell^{1/2} \vec{e} = -j\omega\mu_0 D_\ell^{1/2} D_{\tilde{A}} \vec{j} - D_\ell^{1/2} A^T D_{\tilde{\ell}} D_\mu^{-1} \vec{m}. \quad (13)$$

PML formulation for mesh truncation

The mesh is truncated using perfectly matched layers (PML) that absorb electromagnetic waves following the general ideas of Berenger (1994). The PML is a representation of anisotropic media satisfying

$$\mathbf{D} = \overline{\epsilon}_{\text{PML}} \cdot \mathbf{E} \quad \text{and} \quad \mathbf{B} = \overline{\mu}_{\text{PML}} \cdot \mathbf{H}, \quad (14)$$

where

$$\overline{\epsilon}_{\text{PML}} = \overline{\epsilon} \cdot \overline{\Lambda} \quad \text{and} \quad \overline{\mu}_{\text{PML}} = \overline{\mu} \cdot \overline{\Lambda}. \quad (15)$$

The symbol $\overline{\Lambda}$ stands for a diagonal dyad that has entries selected to absorb incident electromagnetic waves. The form of this dyadic quantity is determined by the normal to the PML interface. As an example, for a PML interface with a normal in the z direction, the form of $\overline{\Lambda}$ is given by Kuzuoglu and Mittra (1996) and by Wu *et al.* (1997) as

$$\overline{\Lambda}_z = \begin{bmatrix} a & 0 & 0 \\ 0 & a & 0 \\ 0 & 0 & 1/a \end{bmatrix}, \quad (16)$$

in which a is given by

$$a = 1 + \frac{f(x,y,z)}{1 + j\alpha\omega}, \quad (17)$$

where α is a constant and $f(x,y,z)$ is a function of position that falls to zero at the interface between the modeling space and the desired PML boundary. We have found through empirical studies that a suitable form for a is

$$a = 1 + \frac{f(x,y,z)}{1 + j\epsilon_0\omega}, \quad (18)$$

where $f(x,y,z)$ is given by

$$f(x,y,z) = \frac{(1-j)\,\beta}{\rho(x,y,z)}. \quad (19)$$

Here, $\rho(x,y,z)$ is a discretized distance from the modeling space/PML interface to the centroid of the cell of interest inside the PML. The parameter β is chosen to fix the amplitude of $f(x,y,z)$.

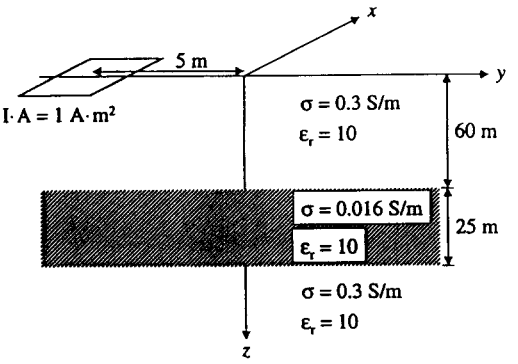

Fig. 2: Current loop at the surface of medium with a buried resistive layer. The same basic picture also applies to our second example with a buried conducting layer, but the conductivity values are reversed (0.3 ↔ 0.016) in that case.

Examples

To demonstrate the accuracy and convergence properties of the code FDFD (for finite-difference/frequency-domain), we have tested various cases against results found in the literature, such as Zhdanov and Feng (1996). These tests will be described elsewhere.

The two sets of examples we will show here are based on the field geometry of Figure 2. Receivers are down a borehole in a layered medium with air above the free surface. The first example of a buried resistive layer has a 60m thick layer with conductivity = 0.3 S/m, a 25m thick layer with conductivity = 0.016 S/m, and a 60m layer with conductivity = 0.3 S/m at the bottom of the model. Appropriately designed PML absorbing layers surround the modeled region on all six sides of the domain. Relative permittivity of all three earth layers is constant and assumed to equal 10.0. The frequency of the excitation is f = 1 kHz with the transmitter located at the free surface with an offset of 5m from the borehole. The finite difference representation was chosen so the unit spacing in the earth model was 2.5m, with 50 cells × 50 cells in the xy direction, and 10 layers of PML on those four sides. In the vertical direction, there were 68 cells in the earth model, 10 cells in the air above the free surface, and 10 more cells above and below for the PML layers. All PML cells are 10m thick in the directions away from the earth model. The overall problem is then approximately $70 \times 70 \times 100 \simeq 500{,}000$ cells. The computations were performed on a DEC Digital Ultimate Workstation (533 MHz), and required approximately 1 hour of CPU time using about 350 iterations to achieve the convergence for

the largest choice of tolerance (10^{-5}). The smallest tolerance (10^{-7}) required about 3.5 hours and 1200 iterations. This computation was serial and required about 500 MB of memory. In Figures 3 and 4 the results of the code calculations for the magnetic field magnitude and phase are compared to results for the same model obtained using the code EM1D (based on a semianalytical formula for such layered models) developed by Ki-Ha Lee at LBNL. The observed agreement is good for all choices of convergence tolerance, but becomes excellent for the two smaller values.

Since the buried resistive layer might be viewed as an easy case for the PML since the majority of the medium is conducting and therefore helping to attenuate the signal — perhaps obviating the need for the PML, we have also tested the code for the reverse problem of a buried conductive layer in a resistive background. All the other parameters are the same including those used for the PML. The computation was performed as in the previous example and required approximately 3.75 hours of CPU time using about 1300 iterations to achieve convergence with observed excellent agreement for the intermediate choice of tolerance (10^{-6}). The smallest tolerance (10^{-7}) required about 4.5 hours and 1600 iterations. In Figures 5 and 6 the results of the code calculations for the magnetic field magnitude and phase are again compared to results for the same model obtained using the code EM1D developed by Ki-Ha Lee at LBNL. The observed agreement is excellent for the two smaller choices of convergence tolerance, but the resistive background case clearly is harder to compute since the worst agreement seen here is for the phase at large depths when the largest choice of convergence tolerance (10^{-5}) was in use.

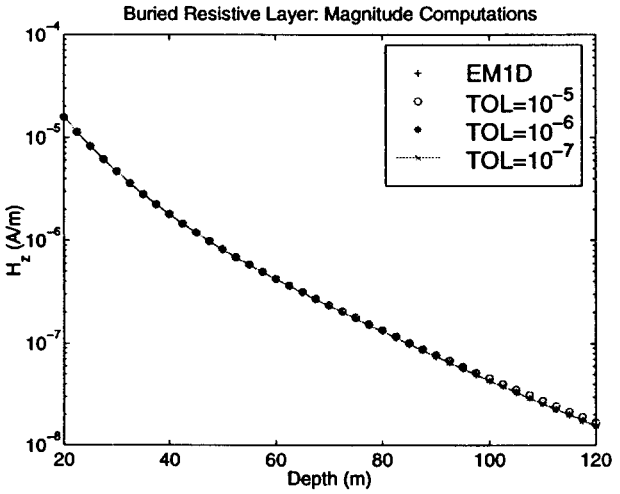

Fig. 3: Comparison of FDFD computed magnitude of magnetic field in the layered model with buried resistive layer in Figure 2 with semianalytic results from EM1D of Ki-Ha Lee (LBNL). The two smaller choices of convergence tolerance give virtually the same results for this example, and are in good agreement with EM1D.

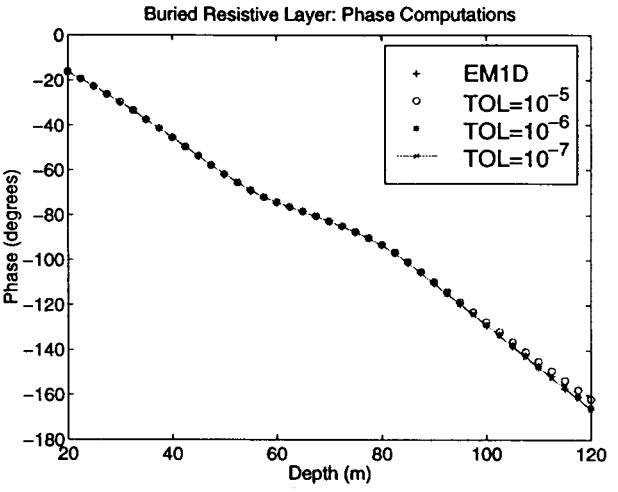

Fig. 4: Comparison of FDFD computed phase of magnetic field in the layered model with buried resistive layer in Figure 2 with semianalytic results from EM1D of Ki-Ha Lee (LBNL). The smallest choice of convergence tolerance gives virtually the same results as EM1D for this example, while the other two are also in good agreement.

Discussion

We continue to test and improve the EM forward modeling capability developed here with the ultimate goal of providing the forward modeling tools needed for a fully nonlinear inversion technique for electromagnetic induction tomography. Working in parallel, a new approach to the inverse problem of electromagnetics has been developed by Dorn *et al.* (1999) based on the so-called "adjoint technique." This method has the very useful property that the inverse problem can be solved approximately by making two uses of the same forward modeling code we have developed and described here. Using a somewhat oversimplified description of this technique, the updates to the electrical conductivity distribution are obtained by first making one pass through the forward solver using the latest best guess of the nature of the conducting medium, and then another pass with the adjoint operator (which for this problem is just the conjugate transpose of the forward modeling operator) applied to the differences in computed and measured data. (The adjoint method is modular when applied in this fashion and could make use of other forward solvers as long as they share the main features of the one described here.) Then the results of these two calculations are combined to determine updates to the original conductivity model. The resulting procedure is iterative and can be applied successively to parts of the data, *e.g.*, data associated with one transmitter location can be used to update the model before other transmitter locations are considered. This procedure has several of the same advantages as the very well tested

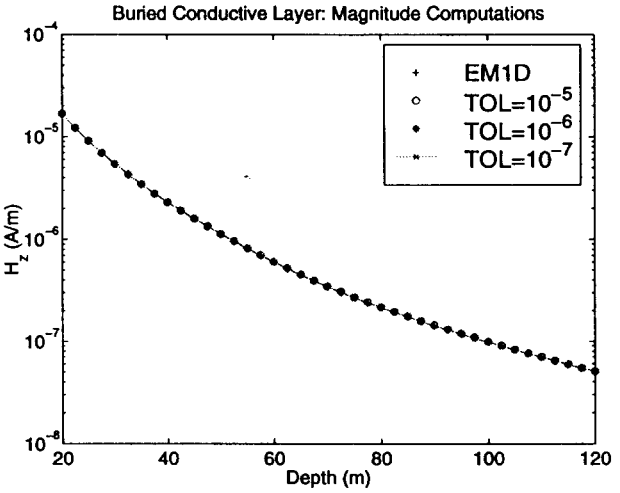

Fig. 5: Comparison of FDFD computed magnitude of magnetic field in the layered model with buried conductive layer as in Figure 2 (but reversing the values $0.3 \leftrightarrow 0.016$) with those from EM1D. All three choices of convergence tolerance give virtually the same results for this example, and are in good agreement with EM1D.

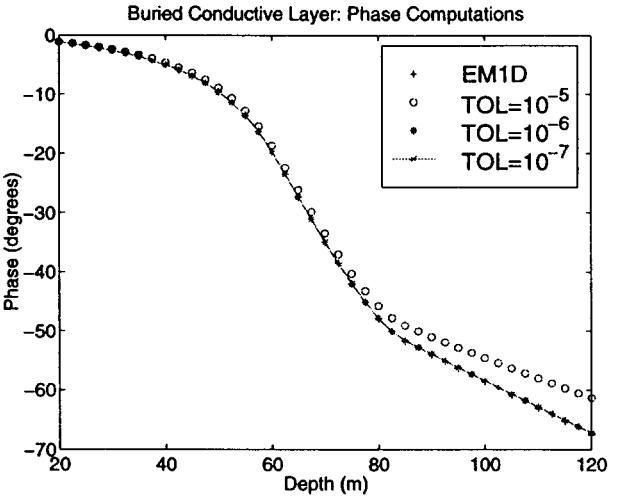

Fig. 6: Comparison of FDFD computed phase of magnetic field in the layered model with buried resistive layer in Figure 2 (but reversing the values $0.3 \leftrightarrow 0.016$) with those from EM1D. The largest deviation from EM1D is observed here for the largest choice of convergence tolerance, while the two smaller values give virtually the same results as EM1D for this example.

method of wave equation migration in reflection seismology (Claerbout, 1975) and is also related to more recent methods in electromagnetics introduced by Zhdanov *et al.* (1996).

Acknowledgments

We thank J. B. Grant and R. M. Sharpe for helping to establish the directions we would take in the EM forward modeling code development for this problem. This work was performed under the auspices of the U.S. Department of Energy by the Lawrence Livermore National Laboratory under contract No. W-7405-ENG-48 and supported specifically by the Environmental Management Science Program of the Office of Environmental Management and the Office of Energy Research.

References

Beilenhoff, K., W. Heinrich, and H. L. Hartnagel, "Improved finite-difference formulation in frequency domain for three-dimensional scattering problems," *IEEE Trans. Microwave Theory Tech.* **40**, 540–546, 1992.

Berenger, J. P., "A perfectly matched layer for the absorption of electromagnetic waves," *J. Computational Phys.* **114**, 185–200, 1994.

Buettner, H. M., and J. G. Berryman, "An electromagnetic induction tomography field experiment at Lost Hills, CA," *SAGEEP Conference Proceedings*, Oakland, California, March 14–18, 1999, pp. 663–672.

Champagne, N. J., II, J. G. Berryman, H. M. Buettner, J. B. Grant, and R. M. Sharpe, "A finite-difference frequency-domain code for electromagentic induction tomography," *SAGEEP Conference Proceedings*, Oakland, California, March 14–18, 1999, pp. 931–940.

Claerbout, J. F., *Fundamentals of Geophysical Data Processing: With Applications to Petroleum Prospecting*, McGraw-Hill, New York, 1976.

Dorn, O., H. Bertete-Aguirre, J. G. Berryman, and G. C. Papanicolaou, "A nonlinear inversion method for 3D-electromagnetic imaging using adjoint fields," *Inverse Problems*, submitted June, 1999.

Kuzuoglu, M., and R. Mittra, "Frequency dependence of the constitutive parameters of causal perfectly matched anisotropic absorbers," *IEEE Microwave Guided Wave Lett.* **6**, 447–449, 1996.

Ramirez, A., W. D. Daily, D. LaBrecque, E. Owen, and D. Chesnut, Monitoring an underground steam injection process using electrical resistance tomography, *Water Resources Res. 29*, 73–87, 1993.

Sacks, Z. S., D. M. Kingsland, R. Lee, and J. F. Lee, "A perfectly matched anisotropic absorber for use as an absorbing boundary condition," *IEEE Trans. Antennas Prop.* **43**, 1460–1463, 1995.

Telford, W. M., L. P. Geldart, R. E. Sheriff, and D. A. Keys, *Applied Geophysics*, Cambridge University Press, Cambridge, England, 1976, Section 3.5.4.

Torres-Verdin, C., and T. M. Habashy, "Rapid 2.5-dimensional forward modeling and inversion via a new nonlinear scattering approximation," *Radio Sci.* **29**, 1051–1079, 1994. Tseng, H.-W., A. Becker, M. J. Wilt, and M. Deszcz-Pan, "A borehole-to-surface electromagnetic survey," *Geophysics* **73**, 1565–1572, 1998.

van der Vorst, H. A., "Bi-CGSTAB: A fast and smoothly converging variant of Bi-CG for the solution of non-symmetric linear systems," *SIAM J. Sci. Stat. Comput.* **12**, 631–644, 1992.

Wu, J. Y., D. M. Kingsland, J. F. Lee, R. Lee, "A comparison of anisotropic PML to Berenger's PML and its application to the finite-element method for EM scattering," *IEEE Trans. Antennas Propagat.* **45**, 40–50, 1997.

Zhdanov, M. S., and S. Feng, "Quasi-linear approximation in 3D electromagnetic modeling," *Geophysics* **61**, 646–665, 1996.

Zhdanov, M. S., P. Traynin, and J. R. Booker, "Underground imaging by frequency-domain electromagentic migration," *Geophysics* **61**, 666–682, 1996.

Zhdanov, M. S., I. M. Varentsov, J. T. Weaver, N. G. Golubev, and V. A. Krylov, "Methods for modeling electromagnetic fields: Results from COMMEMI — The international project on the Comparison Of Modeling Methods for ElectroMagnetic Induction," *J. Appl. Geophys.* **37**, 133–271, 1997.

Appendix

Various special symbols used in this paper will now be defined. First, x_m, y_m, and z_m are the edge lengths of the mth cell (Figure 1) in the x, y, and z directions, respectively. Additional lengths associated with the magnetic fields (staggered grid cell lengths) are given by

$$\overline{x}_m = \frac{(x_m + x_d)}{2}, \overline{y}_m = \frac{(y_m + y_l)}{2}, \overline{z}_m = \frac{(z_m + z_f)}{2}. \quad (20)$$

Then, the area of the staggered grid cell face is given by

$$\begin{aligned} a_{m_x} &= \frac{y_m z_m + y_l z_l + y_f z_f + y_{lf} z_{lf}}{4}, \\ a_{m_y} &= \frac{x_m z_m + x_d z_d + x_f z_f + x_{df} z_{df}}{4}, \\ a_{m_z} &= \frac{x_m y_m + x_d y_d + x_l y_l + x_{dl} y_{dl}}{4} \end{aligned} \quad (21)$$

in the x, y, and z directions, respectively. Next, the permittivities associated with the electric field at an edge are given by

$$\begin{aligned} \overline{\epsilon}_{m_{xx}} &= \frac{y_m z_m \epsilon_{m_{xx}} + y_l z_l \epsilon_{l_{xx}} + y_f z_f \epsilon_{f_{xx}} + y_{lf} z_{lf} \epsilon_{lf_{xx}}}{4}, \\ \overline{\epsilon}_{m_{yy}} &= \frac{x_m z_m \epsilon_{m_{yy}} + x_d z_d \epsilon_{d_{yy}} + x_f z_f \epsilon_{f_{yy}} + x_{df} z_{df} \epsilon_{df_{yy}}}{4}, \\ \overline{\epsilon}_{m_{zz}} &= \frac{x_m y_m \epsilon_{m_{zz}} + x_d y_d \epsilon_{d_{zz}} + x_l y_l \epsilon_{l_{zz}} + x_{dl} y_{dl} \epsilon_{dl_{zz}}}{4}. \end{aligned} \quad (22)$$

And finally, the magnetic permeabilities associated with the magnetic field component at a face are given by

$$\begin{aligned} \overline{\mu}_{m_{xx}} &= \frac{\mu_{m_{xx}} \mu_{d_{xx}} (x_m + x_d)}{(x_m \mu_{d_{xx}} + x_d \mu_{m_{xx}})}, \\ \overline{\mu}_{m_{yy}} &= \frac{\mu_{m_{yy}} \mu_{l_{yy}} (y_m + y_l)}{(y_m \mu_{l_{yy}} + y_l \mu_{m_{yy}})}, \\ \overline{\mu}_{m_{zz}} &= \frac{\mu_{m_{zz}} \mu_{f_{zz}} (z_m + z_f)}{(z_m \mu_{f_{zz}} + z_f \mu_{m_{zz}})}. \end{aligned} \quad (23)$$

The set of all these cell quantities is represented using matrices as

$$\begin{aligned} \boldsymbol{D}_\ell &= \mathrm{Diag}\left(\ldots, z_m, y_m, z_m, \ldots\right), \\ \boldsymbol{D}_{\overline{\ell}} &= \mathrm{Diag}\left(\ldots, \overline{z}_m, \overline{y}_m, \overline{x}_m, \ldots\right), \end{aligned} \quad (24)$$

$$\begin{aligned} \boldsymbol{D}_A &= \mathrm{Diag}\left(\ldots, x_m y_m, x_m z_m, y_m z_m, \ldots\right), \\ \boldsymbol{D}_{\overline{A}} &= \mathrm{Diag}\left(\ldots, a_{m_x}, a_{m_y}, a_{m_z}, \ldots\right), \end{aligned} \quad (25)$$

$$\begin{aligned} \boldsymbol{D}_{A\epsilon} &= \mathrm{Diag}\left(\ldots, \overline{\epsilon}_{m_{xx}}, \overline{\epsilon}_{m_{yy}}, \overline{\epsilon}_{m_{zz}}, \ldots\right), \\ \boldsymbol{D}_\mu &= \mathrm{Diag}\left(\ldots, \overline{\mu}_{m_{xx}}, \overline{\mu}_{m_{yy}}, \overline{\mu}_{m_{zz}}, \ldots\right). \end{aligned} \quad (26)$$

Additionally, the volume matrix is given by

$$\boldsymbol{D}_{V\epsilon\epsilon} = \mathrm{Diag}\left(\ldots, V_{m_x}, V_{m_y}, V_{m_z}, \ldots\right), \quad (27)$$

where

$$\begin{aligned} V_{m_\alpha} = \\ \frac{1}{8}\Big[&|\epsilon_{m_{\alpha\alpha}}|^2 x_m y_m z_m + |\epsilon_{d_{\alpha\alpha}}|^2 x_d y_d z_d + \\ &|\epsilon_{l_{\alpha\alpha}}|^2 x_l y_l z_l + |\epsilon_{f_{\alpha\alpha}}|^2 x_f y_f z_f + \\ &|\epsilon_{df_{\alpha\alpha}}|^2 x_{df} y_{df} z_{df} + |\epsilon_{dl_{\alpha\alpha}}|^2 x_{dl} y_{dl} z_{dl} + \\ &|\epsilon_{lf_{\alpha\alpha}}|^2 x_{lf} y_{lf} z_{lf} + |\epsilon_{dlf_{\alpha\alpha}}|^2 x_{dlf} y_{dlf} z_{dlf}\Big]. \end{aligned} \quad (28)$$

The vectors $\vec{e}$, $\vec{h}$, $\vec{j}$, and $\vec{m}$ have the general form

$$\vec{f} = \left(\ldots, F_{m_x}, F_{m_y}, F_{m_z}, \ldots\right). \quad (29)$$

Finally, the coefficient matrices $\boldsymbol{A}$ and $\boldsymbol{B}$ are given in Champagne *et al.* (1999).

University of California
Lawrence Livermore National Laboratory
Technical Information Department
Livermore, CA 94551

236779

NOV 08 1999

This report was prepared as an account of Government sponsored work. Neither the United States, nor the Commission, nor any person acting on behalf of the Commission:

A. Makes any warranty or representation, expressed or implied, with respect to the accuracy, completeness, or usefulness of the information contained in this report, or that the use of any information, apparatus, method, or process disclosed in this report may not infringe privately owned rights; or

B. Assumes any liabilities with respect to the use of, or for damages resulting from the use of any information, apparatus, method, or process disclosed in this report.

As used in the above, "person acting on behalf of the Commission" includes any employee or contractor of the Commission, or employee of such contractor, to the extent that such employee or contractor of the Commission, or employee of such contractor prepares, disseminates, or provides access to, any information pursuant to his employment or contract with the Commission, or his employment with such contractor.